

Ergodic Trajectory Planning with Dynamic Sensor Footprints

Ziyue Zheng¹, Yongce Liu¹, Hesheng Wang¹, Zhongqiang Ren^{1†}

Abstract—This paper addresses the problem of trajectory planning for information gathering with a dynamic and resolution-varying sensor footprint. Ergodic planning offers a principled framework that balances exploration (visiting all areas) and exploitation (focusing on high-information regions) by planning trajectories such that the time spent in a region is proportional to the amount of information in that region. Existing ergodic planning often oversimplifies the sensing model by assuming a point sensor or a footprint with constant shape and resolution. In practice, the sensor footprint can drastically change over time as the robot moves, such as aerial robots equipped with downward-facing cameras, whose field of view depends on the orientation and altitude. To overcome this limitation, we propose a new metric that accounts for dynamic sensor footprints, analyze the theoretic local optimality conditions, and propose numerical trajectory optimization algorithms. Experimental results show that the proposed approach can simultaneously optimize both the trajectories and sensor footprints, with up to an order of magnitude better ergodicity than conventional methods. We also deploy our approach in a multi-drone system to ergodically cover an object in 3D space.

I. INTRODUCTION

This paper investigates a trajectory planning problem for area search, which arises in applications such as search and rescue [1] and target localization [2]. Given an information map and a probability distribution in the area to be searched, the problem requires planning a trajectory to gather information from this information map efficiently. Existing approaches to solve this problem span a spectrum that ranges from information-theoretic approaches [3], [4], which greedily move the robot to the next location with the highest information gain, to uniform coverage methods [3], [5], which guarantee complete exploration of the entire information map. In the middle of this spectrum lies the ergodic search [6]–[8], which plans trajectories by optimizing an ergodic metric so that, along the planned trajectory, the amount of time spent in a region is proportional to the amount of information in that region. Ergodic search provides a framework to inherently balance between exploration (i.e., attempting to visit all possible locations for new information) and exploitation (i.e., myopically searching high-information areas) and is thus able to intelligently plan the robot motion to gather information in the long run.

Existing ergodic search methods typically simplify the sensor detection range (i.e., sensor footprint), which describes the footprint as either a single point [6], [7], [9] in the workspace or a circle with a constant radius [10]. In practice,

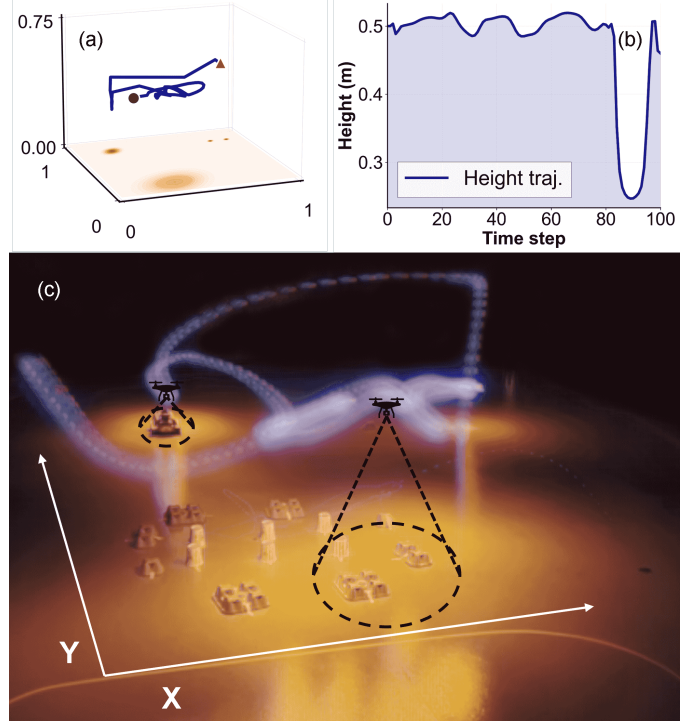


Fig. 1. Demonstration with a drone. (a) and (b) show the trajectory planned by our planner and the corresponding height values (z coordinate) of the robot along the trajectory. (c) shows the execution of the trajectory with a real drone equipped with a downward pointing LED to visualize the dynamic sensor footprint whose size depends on the flying height of the robot. With our approach, the robot flies high over regions with widespread information and flies low over regions with concentrated information. The orange shadow on the ground in (c) visualizes the time-averaged statistics of the dynamic sensor footprint, which is similar to the information map to be covered as shown in (a).

the sensor footprint often varies as the robot moves. For example, consider a drone with a camera that points downward to the ground to collect information (Fig. 1). The field of view forms a cone. The sensor footprint projected onto the ground is therefore a circle whose radius changes with the drone's altitude. Moreover, the footprint size correlates negatively with the sensor resolution: At higher altitudes, the footprint is larger and the resolution is coarser, collecting rough information over a broad area; At lower altitudes, the footprint is smaller and the resolution is finer, detecting concentrated, detailed information within small regions.

To capture these dynamic sensing characteristics, this paper seeks to integrate a dynamically changing sensor footprint and

[†] The authors are at Shanghai Jiao Tong University in China, Correspondence: zhongqiang.ren@sjtu.edu.cn

resolution into the ergodic search framework. To this end, we describe the sensor footprints along a robot trajectory as a random process and introduce a *footprint ergodic metric* which computes the time-averaged statistics of the dynamic sensor footprints and compares it against the information map to be covered. The proposed footprint ergodic metric converges to the existing ergodic metric [6] as the sensor footprint approaches a single point in the limit. With the proposed footprint ergodic metric, we formulate a corresponding ergodic optimal control problem (OCP) and rewrite this OCP into standard Bolza forms, which then allows us to leverage the Pontryagin minimum principle to derive the theoretical local optimality conditions for the OCP. In practice, the proposed footprint ergodic metric involves an integration that can be inefficient to compute, and we therefore propose a numerical method to compute it approximately based on a finite number of samples. As the number of samples increases and approaches infinity, our numerical approximation converges to the true footprint ergodic metric. Finally, to incorporate more sophisticated constraints from practice, we leverage both the numerical footprint ergodic metric and the Augmented Lagrangian to plan the trajectories, and we name this approach Footprint Ergodic Optimization (FEO).

To evaluate our approach, we compare our method on various information maps in simulation against several baselines, including conventional ergodic search and ergodic search with fixed footprint. We also deploy our approach on a multi-drone system in a lab setting to ergodically cover both a 2D information map and an object in 3D. The experimental results show that, our method outperforms these baselines due to the ability to dynamically adjust the sensor footprint when planning the robots' motion. Intuitively, the drone tends to fly further away from the surface in regions with low-density information, and closer to the surface in areas with concentrated information. Our approach achieves up to near an order of magnitude better ergodicity compared to the best-performing baseline.

II. RELATED WORK

A. Ergodic Search

Ergodic search plans trajectories by minimizing the difference between the robot's time-averaged statistics and the workspace's information distribution. Several approaches have been proposed to evaluate the difference, including spectral multi-scale coverage using Fourier analysis [6], Kullback–Leibler divergence with Gaussian mixture models [11], kernel ergodic metric for Lie group spaces [12], and maximum mean discrepancy metric [13]. For trajectory optimization, gradient-based methods are widely adopted. Some techniques involve feedback control for dynamic systems [6], receding-horizon planning [2], potential field approaches [14], and LQR-based optimization [7]. Recent developments have incorporated additional considerations like time efficiency [15], multi-objective criteria [16], and probabilistic inter-robot connectivity [17]. Ergodic search is also validated in robotic manipulation [18] and target localization [2]. However, existing studies either ignore the impact of robot sensor footprint

on information gathering, or only consider fixed size sensor footprint during the robot motion.

B. Ergodic Coverage of 3D Targets

Although being generic to the general workspace, most experiments on ergodic search are limited to a 2D workspace [6], [9], [17]. Very recently, some work investigates ergodic search in 3D workspace, such as the coverage of non-planar surfaces in object inspection or surface scanning with robotic arms [19], [20]. Some of these methods discretize the target surfaces and allows the ergodic metric [6] to be computed over manifolds, which enables coverage planning on non-planar surfaces of a 3D target [19]. Others use heat equation-driven area coverage [20], [21] to optimize end-effector trajectories to match a desired spatial distribution. However, these approaches still consider simplified sensor footprint such as point or fixed size circle. This work also tests the proposed approach for target coverage in 3D with dynamic sensor footprints using a multi-drone system.

C. Dynamic Sensor Footprints

For information gathering problems, sensors and information gathering are investigated in many areas, such as sensor coverage for planning [22]–[26], sensor view points in SLAM, target detection and tracking [27]–[32]. However, most of them simplify the sensor as a point in the workspace and ignore the detection range and resolution of the sensor [33], or as a fixed geometry such as circles [10], rectangles [32], [34], or spheres [23] without considering that the sensor detection range and resolution vary with robot dynamics. Few works consider varying sensor footprints and focus mainly on uniform coverage [35], [36] or environmental monitoring with different resolutions [37], as opposed to ergodic optimal control considered in this paper.

III. PRELIMINARIES

A. Workspace and Trajectories

Let $\mathcal{W} = [0, L_1] \times \cdots \times [0, L_\nu]$, $\nu = 2, 3$ denote a bounded ν -dimensional workspace, which is to be explored by the robot.¹ The robot has an n -dimensional state space ($n \geq \nu$), and let $x : [0, T] \rightarrow \mathbb{R}^n$ denote a trajectory in the state space with $T \in \mathbb{R}^+$ representing the time horizon. At any time $t \in [0, T]$, the state of the robot $x(t)$ must stay within the set $\mathcal{X} \subseteq \mathbb{R}^n$, which is a set of allowed states. Here, \mathcal{X} describes the constraints on the robot's state, such as avoiding collision with the static obstacles in the workspace or staying within the bounded workspace. The robot has deterministic dynamics given by $\dot{x}(t) = f_d(x(t), u(t))$, where $u(t) \in \mathcal{U}$ is the control input of the robot. Let $f_q : \mathbb{R}^n \rightarrow \mathcal{W}$ denote a map that projects a state $x(t)$ to the corresponding point $q(t) \in \mathcal{W}$ in the workspace, i.e., $q(t) = f_q(x(t))$.

¹The workspace in this paper is simply the space of information to be explored by the robot, and the robot can move in a higher-dimensional space than the workspace. For example, the robot can be a drone flying in 3D space while exploring the information in a 2D workspace.

B. Ergodic Metric

Let $\phi(w) : \mathcal{W} \rightarrow \mathbb{R}_0^+$ denote an information map over the workspace, which is a time-invariant probability distribution function with $\int_{\mathcal{W}} \phi(w) dw = 1$, describing the information density at each point in the workspace \mathcal{W} . Based on the trajectory $q(t)$, the time-averaged statistics for the robot is defined as follows [6].

$$c(w, x(t)) = c(w, f_q(x(t))) = \frac{1}{T} \int_0^T \delta(w - q(t)) dt \quad (1)$$

where $\delta(w)$ is the Dirac delta function such that $\delta(0) = +\infty$ and $\delta(w) = 0, w \neq 0$, satisfying $\int_{\mathcal{W}} \delta(w) dw = 1$.

With the information distribution $\phi(w)$ and the time-averaged statistics (1), the ergodic metric (ergodicity) is defined as follows [6].

$$\begin{aligned} \mathcal{E}(\phi, q(t)) &= \sum_{\mathbf{k} \in \mathcal{K}} \Lambda_{\mathbf{k}} (c_{\mathbf{k}} - \phi_{\mathbf{k}})^2 \\ &= \sum_{\mathbf{k} \in \mathcal{K}} \Lambda_{\mathbf{k}} \left(\frac{1}{T} \int_0^T F_{\mathbf{k}}(q(t)) dt - \int_{\mathcal{W}} \phi(w) F_{\mathbf{k}}(w) dw \right)^2 \end{aligned} \quad (2)$$

Here, $c_{\mathbf{k}}$ and $\phi_{\mathbf{k}}$ are the Fourier coefficients of $c(w)$ and $\phi(w)$, respectively. $\mathbf{k} = (k_1, \dots, k_\nu) \in \mathcal{K}$ is the frequency vector of the Fourier coefficients, and $\mathcal{K} \subset \mathbb{N}^\nu$ represents a selected set of frequencies in practical computation. Additionally, $F_{\mathbf{k}}(w) = \frac{1}{h_{\mathbf{k}}} \prod_{o=1}^\nu \cos \frac{k_o \pi}{L_o} w_o$ is the cosine basis function with the normalization term $h_{\mathbf{k}}$ [6], [15], [38]. $\Lambda_{\mathbf{k}} = (1 + \|\mathbf{k}\|_2^2)^{-(\nu+1)/2}$ is the weight of each Fourier coefficient.

C. Ergodic Trajectory Optimization Problem

Given an information map ϕ , the goal of the Ergodic Trajectory Optimization (ETO) problem is to find a dynamically feasible trajectory x of the robot that minimizes the ergodic metric $\mathcal{E}(\phi, q)$ and control effort:

$$\min_{x, u} \mathcal{E}(\phi, q) + \int_0^T u^T(t) R u(t) dt \quad (3a)$$

$$\text{s.t. } \dot{x} = f_d(x(t), u) \quad (3b)$$

$$x \in \mathcal{X}, u \in \mathcal{U} \quad (3c)$$

where R is a positive definite matrix describing the weight of the controls. Constraint 3b represents the dynamics of the robot, and 3c defines the constraints of state and control.

IV. METHOD

A. Footprint Ergodic Metric

Definition 1 (Sensor Footprint). Let $\gamma(w, x) \subset \mathcal{W}, w \in \mathcal{W}$ denote the sensor footprint of the robot (over the information map in the workspace) when the robot state is x , satisfying $\int_{\mathcal{W}} \gamma(w, x) dw = 1$ and $\gamma(w, x) > 0, \forall w \in \mathcal{W}$.

Intuitively, when the robot state is x , for any point in the workspace $w \in \mathcal{W}$, $\gamma(w, x)$ returns the “weight of measurement” at point w , and the weight integrated at all possible points $w \in \mathcal{W}$ should be equal to one. In other words, $\gamma(w, x)$ can be regarded as a probability distribution

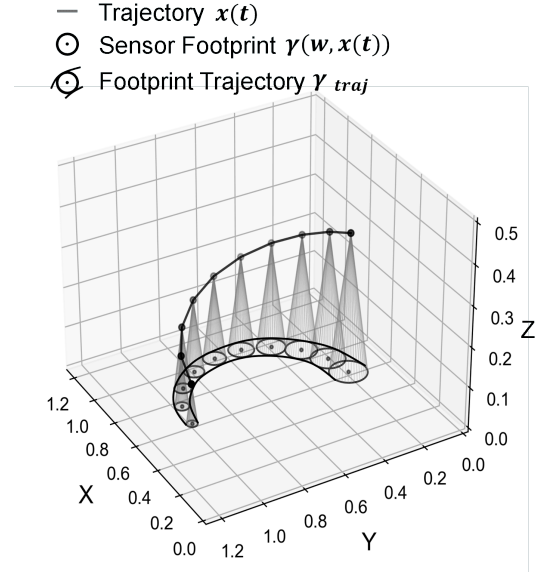


Fig. 2. Illustration of sensor footprint and footprint trajectory of a flying drone with downwards pointing camera over a 2D information map.

over the workspace \mathcal{W} that depends on the parameter x , and $\gamma(w = w', x(t_k))$ is the value of the probability density function at a specific point $w' \in \mathcal{W}$.

Example 1. Consider a 2D workspace ($\nu = 2$) to be explored by a flying robot with a downward pointing camera whose optic axis is always perpendicular to the workspace. The sensor footprint can be described by a uniform circle, whose radius depends on the flying height of the robot. Specifically, for each robot state trajectory x , let $f_h : \mathbb{R}^n \rightarrow \mathbb{R}^+$ denote a map that projects a state $x(t)$ to a positive real number $h(t)$ representing the height of the robot, i.e., $h(t) = f_h(x(t))$. Then, the sensor footprint $\gamma(w, x)$ can be described by the following uniform distribution within the circle (Fig. 2).

$$\gamma(w, x(t)) = \begin{cases} \frac{1}{\pi k_h^2 f_h(x)^2} & \text{if } \|w - f_q(x)\|_2 \leq k_h f_h(x) \\ 0 & \text{otherwise} \end{cases} \quad (4)$$

where $k_h \in \mathbb{R}^+$ is a known constant related to the downward viewing angle of the robot.²

When the robot moves along a trajectory $x(t), t \in [0, T]$, the corresponding sensor footprint varies along $x(t)$.

Definition 2 (Footprint Trajectory (FT)). Let $\gamma(w, x(t))$ denote a sensor footprint trajectory, where for each time point $t_k \in [0, T]$, $\gamma(w, x(t_k))$ is a sensor footprint.

Fig. 2 provides an illustration of footprint trajectory over a 2D information map. Since at any time point $t_k \in [0, T]$, $\gamma(w, x(t_k))$ is a probability distribution over the workspace, an FT $\gamma(w, x(t))$ is actually a random process. We will sample from this random process to develop a numerical approach for easy computation as presented later.

²To simplify the presentation, this work assumes the entire footprint is always inside the workspace, i.e., $f_q(x)$ is inside \mathcal{W} and is at least $k f_h(x)$ away from the nearest boundary of \mathcal{W} . In practice, this can be ensured by adding constraints on the robot's state as described by $x \in \mathcal{X}$.

Similar to the time-averaged statistics of a robot trajectory $c(w, x)$ as mentioned in Eq. 1, we then introduce the time-averaged statistics of an FT $\gamma(w, x(t))$.

Definition 3 (Time-Averaged Statistics of FT). *Let $c_\gamma(w, x(t))$, $w \in \mathcal{W}$, $f_q(x(t)) \in \mathcal{W}$ denote the time-averaged statistics of an FT $\gamma(w, x(t))$:*

$$c_\gamma(w, x(t)) = \frac{1}{T} \int_0^T \gamma(w, x(\tau)) d\tau, \quad (5)$$

Intuitively, Eq. 5 replaces the delta function δ in Eq. 1 with the footprint trajectory γ . To simplify the notation, we omit t in $x(t)$ and write $c_\gamma(w, x(t))$ as $c_\gamma(w, x)$.

An ergodic metric between $c_\gamma(w, x(t))$ and an information map ϕ can then be defined in a similar way as in Eq. 2.

Definition 4 (Footprint Ergodic Metric). *Let \mathcal{E}_γ denote the Footprint Ergodic Metric:*

$$\begin{aligned} \mathcal{E}_\gamma(\phi, x) &= \sum_{\mathbf{k} \in \mathcal{K}} \Lambda_{\mathbf{k}} (c_{\gamma, \mathbf{k}} - \phi_{\mathbf{k}})^2 \\ &= \sum_{\mathbf{k} \in \mathcal{K}} \Lambda_{\mathbf{k}} \left(\int_{\mathcal{W}} c_\gamma(w, x) F_{\mathbf{k}}(w) dw - \int_{\mathcal{W}} \phi(w) F_{\mathbf{k}}(w) dw \right)^2 \end{aligned} \quad (6)$$

Here, $c_{\gamma, \mathbf{k}}$ are the Fourier coefficients of $c_\gamma(w, x)$ for $\mathbf{k} \in \mathcal{K}$.

The following theorem shows the relationship between the proposed footprint ergodic metric and the conventional ergodic metric [6]. Let $B(\gamma)$ denote a bounding sphere of $\gamma = \gamma(w, x)$ such that for any point $w' \notin B(\gamma)$, $\gamma(w', x) = 0$. In other words, γ can only take non-zero values within $B(\gamma)$. Let $r_B(\gamma)$ denote the radius of $B(\gamma)$. Intuitively, as $r_B(\gamma)$ approaches zero, since $\int_{\mathcal{W}} \gamma(w, x) dw = 1$, the footprint $\gamma(w, x)$ becomes a Dirac delta function at $w = q(x)$.

Theorem 1. *As $r_B(\gamma)$ approaches 0:*

$$\lim_{r_B(\gamma) \rightarrow 0} c_\gamma(w, x(t)) = c(w, x(t)) \quad (7)$$

$$\lim_{r_B(\gamma) \rightarrow 0} \mathcal{E}_\gamma(\phi, x) = \mathcal{E}(\phi, x) \quad (8)$$

Problem 1 (ETO-DF Problem). *Given an information map ϕ , the goal of the Ergodic Trajectory Optimization with Dynamic sensor Footprint (ETO-DF) problem is to find a dynamically feasible trajectory x of the robot that minimizes the footprint ergodic metric $\mathcal{E}_\gamma(\phi, x)$ and the accumulated control effort:*

$$\min_{x, u} \mathcal{E}_\gamma(\phi, x) + \int_0^T u^T(t) R u(t) dt \quad (9)$$

$$\text{s.t. (3b), (3c)} \quad (10)$$

The only difference between ETO-DF and ETO is to replace the ergodic metric \mathcal{E} in the objective function with the footprint ergodic metric \mathcal{E}_γ . All other constraints remain unchanged.

B. Necessary Conditions for Local Optimality

To apply the Pontryagin Minimum Principle to derive the local optimality conditions for ETO-DF, we need to rewrite the ETO-DF problem into the standard Bolza form. However, the term \mathcal{E}_γ depends on the entire state trajectory, which needs to be reformulated as either a stage cost or terminal cost term.

Similar techniques as in [8] for the regular ergodic metric can be adapted here to convert \mathcal{E}_γ into a terminal cost term based on a new definition of state.

Definition 5. (Auxiliary State and Joint State). *Let $s(t) = (s_0(t), s_{(1,0,\dots)}(t), \dots, s_{\mathbf{k}_{|\mathcal{K}|}}(t))$ denote an auxiliary state, where each element $s(t)$ is defined as $\int_{\mathcal{W}} \int_0^t \gamma(w, x(\tau)) F_{\mathbf{k}}(w) d\tau dw - t\phi_{\mathbf{k}}$. Then, we define the joint state as $\bar{x} = [x^T, s^T]^T$, which is subject to the joint dynamic:*

$$\dot{\bar{x}} = \bar{f}_d(\bar{x}, u) = \begin{bmatrix} f_d(x, u) \\ g(x(t)) \end{bmatrix} \quad (11)$$

$$g(x(t)) = \int_{\mathcal{W}} \gamma(w, x(\tau)) F_{\mathbf{k}}(w) dw - \Phi \quad (12)$$

Then the footprint ergodic metric can be expressed as the terminal form of the auxiliary state:

$$\mathcal{E}_\gamma(\phi, x) = \frac{1}{2} s^T(T) Q_{\mathcal{K}} s(T) \quad (13)$$

$$Q = \frac{2}{T^2} \text{diag}(\Lambda_0, \dots, \Lambda_{\mathcal{K}}) \quad (14)$$

with the initial condition $s(0) = \mathbf{0}$. Here, $Q_{\mathcal{K}}$ represents a diagonal matrix constructed from the elements $(s(t))$, and $\Phi = (\phi_0, \dots, \phi_{\mathbf{k}_{|\mathcal{K}|}})$ denotes the Fourier coefficient vector corresponding to the distribution of information. $F_{\mathbf{k}}(w)$ represents the basis functions as aforementioned.

We then define the Lagrange function to convert a constrained optimization problem into an unconstrained one. The Lagrange function of ETO-DF can be written as follows, with Lagrange multipliers $\lambda_x(t) \in \mathbb{R}^n$ for x and $\lambda_s(t) \in \mathbb{R}^{|\mathcal{K}|}$ for s .

$$\begin{aligned} \mathcal{L}(x, u, \lambda) &= \mathcal{E}_\gamma(\phi, x) + \int_0^T u^T(t) R u(t) \\ &+ \lambda_x^T(t) (\dot{x} - f(x(t), u(t))) dt + \lambda_s^T(t) (\dot{s} - g(x(t))) dt \end{aligned} \quad (15)$$

We define the Hamiltonian as:

$$\begin{aligned} \mathcal{H}(x, s, u, \lambda_x, \lambda_s, t) &= u^T(t) R u(t) + \\ &\lambda_x^T f_d(x(t), u(t)) + \lambda_s^T g(x(t)) \end{aligned} \quad (16)$$

Theorem 2. (Necessary Optimality Condition). *For the ETO-DF problem, the necessary conditions for a control law u and the associated state trajectory of the robot x to be locally optimal are:*

$$\dot{x}(t) = \nabla_{\lambda_x} \mathcal{H} \quad \bar{x}(0) = \bar{x}_0 \quad (17a)$$

$$\dot{s}(t) = \nabla_{\lambda_s} \mathcal{H} = g(x) \quad s(0) = \mathbf{0} \quad (17b)$$

$$\dot{\lambda}_x^T(t) = -\nabla_x^T \mathcal{H} \quad (17c)$$

$$\lambda_x^T(T) = 0 \quad (17d)$$

$$\dot{\lambda}_s^T(t) = -\nabla_s^T \mathcal{H} = 0 \quad (17d)$$

$$\lambda_s^T(T) = \frac{\partial \frac{1}{2} s^T(T) Q_{\mathcal{K}} s(T)}{\partial s(T)} \quad (17e)$$

$$\nabla_u^T \mathcal{H} = 0 \quad (17e)$$

$$u^*(t) = \arg \min_{u \in \mathcal{U}} \mathcal{H}(x, u, \lambda, t) \quad (17f)$$

Proof. Using the Hamiltonian (Eq. 16), the Lagrange function (Eq. 15) can be rewritten as:

$$\mathcal{L} = \frac{1}{2} s^T(T) Q_K s(T) + \int_0^T \mathcal{H}(x, s, u, \lambda_x, \lambda_s, t) - \lambda_x^T \dot{x} - \lambda_s^T \dot{s} dt \quad (18)$$

Here, the terminal cost term depends only on the auxiliary system state s and is not influenced by x . As a result, we can derive the optimality conditions by taking the total variational derivative of Eq. 18 for the states x, s , derivatives \dot{x}, \dot{s} , control u , and multipliers λ_x, λ_s .

$$\begin{aligned} \delta \mathcal{L} = & \frac{\partial \frac{1}{2} s^T(T) Q_K s(T)}{\partial s(T)} \delta s(T) \\ & + \int_0^T \{ \nabla_x^T \mathcal{H} \delta x(t) + \nabla_s^T \mathcal{H} \delta s(t) \\ & + \nabla_u^T \mathcal{H} \delta u(t) + \nabla_{\lambda_x}^T \mathcal{H} \delta \lambda_x(t) \\ & + \nabla_{\lambda_s}^T \mathcal{H} \delta \lambda_s(t) - \dot{x}(t)^T \delta \lambda_x(t) - \lambda_x^T(t) \delta \dot{x}(t) \\ & - \dot{s}(t)^T \delta \lambda_s(t) - \lambda_s^T(t) \delta \dot{s}(t) \} dt \end{aligned} \quad (19)$$

Using integration by parts for $\lambda_x^T \delta \dot{x}$ and $\lambda_s^T \delta \dot{s}$, Eq. 19 can be simplified as follows:

$$\begin{aligned} \delta \mathcal{L} = & \left(\frac{\partial \frac{1}{2} s^T(T) Q_K s(T)}{\partial s(T)} - \lambda_s^T(T) \right) \delta s(T) \\ & - \lambda_x^T(T) \delta x(T) + \int_0^T \{ (\nabla_x^T \mathcal{H} + \dot{\lambda}_x^T(t)) \delta x(t) \\ & + (\nabla_s^T \mathcal{H} + \dot{\lambda}_s^T(t)) \delta s(t) + \nabla_u^T \mathcal{H} \delta u(t) + (\nabla_{\lambda_x}^T \mathcal{H} \\ & - \dot{x}(t)^T) \delta \lambda_x(t) + (\nabla_{\lambda_s}^T \mathcal{H} - \dot{s}(t)^T) \delta \lambda_s(t) \} dt \end{aligned} \quad (20)$$

Let $\delta \mathcal{L} = 0$, we can derive the conditions as shown in Eq. 17. To achieve optimality, the trajectory must satisfy the initial conditions for x and s as specified in Eq. 17a and Eq. 17b. The associated costate equations, together with their terminal conditions, are given by Eq. 17c for x and Eq. 17d for s . The multiplier equation in Eq. 17e must be fulfilled. The optimal control input is determined by minimizing the Hamiltonian (Eq. 16), subject to the condition in Eq. 17f. \square

C. Numerical Computation of Footprint Ergodic Metric

To solve ETO-DF numerically, we use direct transcription to convert the continuous-time dynamics and constraints into discrete nonlinear optimization, and then employ an optimization method, such as L-BFGS, to minimize the Lagrange function. This approach also allows us to handle additional constraints as described in the next section on multi-robot. To optimize the Lagrangian, the gradient of Eq. 15 with respect to the state x and control u is required:

$$\frac{\partial \mathcal{L}}{\partial x} = \frac{\partial \mathcal{E}_\gamma(\phi, x)}{\partial x} + \frac{\partial \int_0^T u^T R u + \lambda^T (\dot{x} - f(x, u)) dt}{\partial x} \quad (21)$$

The first term $\frac{\partial \mathcal{E}_\gamma(\phi, x)}{\partial x}$ requires an integration over the sensor footprint to compute \mathcal{E}_γ and then taking the derivative of the integrated value with respect to x , which is complicated especially when the sensor footprint $\gamma(w, x)$ corresponds to

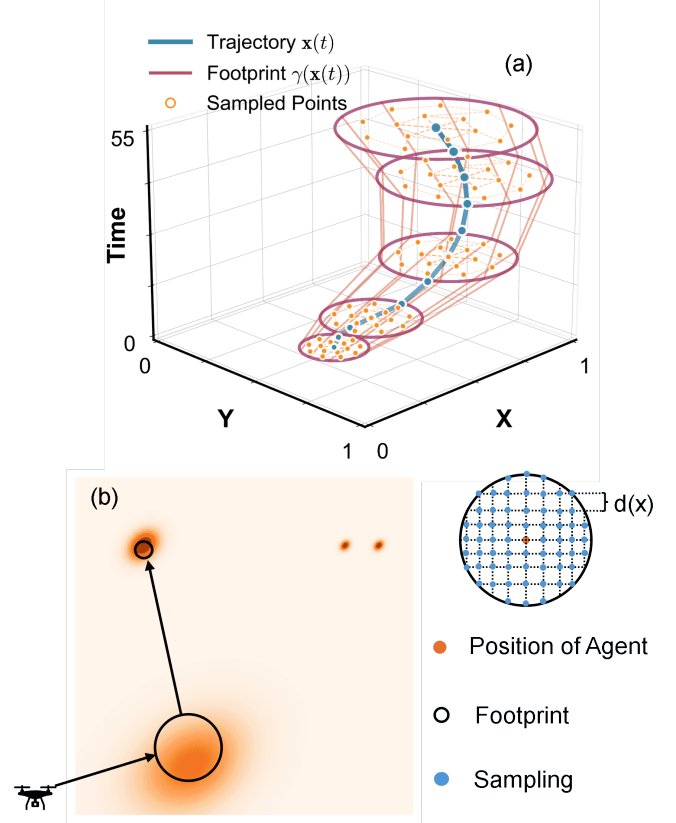


Fig. 3. Numerical computation of the footprint ergodic metric. (a) shows a trajectory of the robot and the corresponding footprint trajectory $\gamma(w, x(t))$, which is a random process. The orange dots in the footprint at each time point represent the set of sampled points at that time. All these points together form W_s , a set of M realizations of the random process $\gamma(w, x(t))$. (b) shows the sampling method we used in this paper as explained in Example 2.

a complex probability distribution. We therefore propose an alternative way to numerically compute the footprint ergodic metric \mathcal{E}_γ approximately.

Let $W_s = \{w_1(t), w_2(t), \dots, w_M(t)\}$ denote a set of M trajectories in the workspace W that are realizations of the random process $\gamma(w, x(t))$. In other words, for any time point $t_k \in [0, T]$, for each realization $w_m \in W_s$, $w_m(t_k)$ is a sampled point from the corresponding random variable $\gamma(w, x(t_k))$ (Fig. 3(a)). Here, each sampled trajectory is not required to be continuous with respect to time. Note that, for an area where $\gamma(w, x(t_k))$ has a higher probability value, more samples $w_m(t_k)$ tend to locate within that area. Then, a footprint trajectory (FT) in Def. 3 can be approximated by the following Approximated FT (A-FT):

$$\gamma'(w, x(t)) = \frac{\sum_{m=1}^M \delta(w - w_m(t))}{M} \quad (22)$$

The time-average statistics of the footprint ergodic metric can be approximated with the help of A-FT:

$$\begin{aligned} c'_\gamma(w, x(t)) &= \frac{1}{T} \int_0^T \gamma'(w, x(\tau)) d\tau \\ &= \frac{1}{TM} \int_0^T \sum_{m=1}^M \delta(w - w_m(t)) d\tau \end{aligned} \quad (23)$$

whose corresponding Fourier coefficients are:

$$c'_{\gamma, \mathbf{k}} = \frac{1}{TM} \int_0^T \sum_{m=1}^M F_{\mathbf{k}}(w_m(t)) dt, \mathbf{k} \in \mathcal{K} \quad (24)$$

Finally, the footprint ergodic metric can be approximated by:

$$\mathcal{E}'_{\gamma}(\phi, x) = \sum_{\mathbf{k} \in \mathcal{K}} \Lambda_{\mathbf{k}} (c'_{\gamma, \mathbf{k}} - \phi_{\mathbf{k}})^2 \quad (25)$$

Example 2. Following Example 1, when the sensor footprint is a uniform distribution, a possible way to sample from the corresponding footprint trajectory γ is to conduct grid-like sampling with adaptive resolution as showing in Fig. 3. Specifically, let a positive real number $d(x) = k_d f_h(x)$ denote the adaptive sampling resolution that varies with the robot state x , where k_d is a parameter that controls the density of samples. Start from the projected position of the robot in the workspace plane, and iteratively draw samples with $d(x)$ distance along the x and y axes until all possible samples within the sensor footprint (Eq. 4) are drawn.

With this numerical method to compute footprint ergodic metric, we can readily obtain all the gradient terms in Eq. 21, which then allows us to use any existing optimization algorithm to solve the problem. We use BFGS to optimize the Lagrangian to solve the problem. We refer to the entire numerical computation process as Footprint Ergodic Optimization (FEO).

D. Multi-Robot Ergodic Coverage in 3D

This section extends the proposed metric and algorithm to multi-agent systems and seeks to ergodically cover an object in 3D. Let $I = \{1, 2, \dots, N_r\}$ denote a set of N_r robots. We use a superscript $i, j \in I$ over a variable to indicate to which robot that variable belongs. For example, x^i, u^i denote the state and control of robot i , respectively. Let $O \subset \mathcal{W} \subset \mathbb{R}^3$ denote an object in the 3D workspace, and let ∂O denote the surface of the object.

1) *Sampling from Surfaces:* Instead of using a 2D mesh to describe the information distribution on the object surface [19], we simply consider an information map $\phi : \mathcal{W} \rightarrow [0, 1]$ defined over the 3D workspace $\mathcal{W} \subset \mathbb{R}^3$ satisfying $\phi(w) = 0, w \notin \partial O$ and $\int_{\mathcal{W}} \phi(w) = 1$. In other words, only for the points $w \in \partial O$ that are on the surface of the object, the information $\phi(w)$ may not be zero.

The sensor footprint $\gamma(w, x) \subset \mathcal{W}$ is a volume in the 3D workspace by Def. 1. Since there is no information for any point not on the surface of the object, we can set $\gamma(w, x) = 0, w \notin \partial O$. In other words, we only need to consider the surface of the object that is covered by the sensor, i.e., a subset of the footprint that intersects with the object surface. When computing the approximated time-averaged statistics of the footprint ergodic metric c'_{γ} as defined in Eq. 24, we only need to sample points from the subset of the object surface that is covered by the sensor footprint.

As illustrated in Fig. 4, one possible way for sampling is to sample a set of rays starting from the position of the robot $q(t) = f_q(x(t))$ pointing outwards inside the sensor footprint. For each of those rays, ray tracing can help find the point

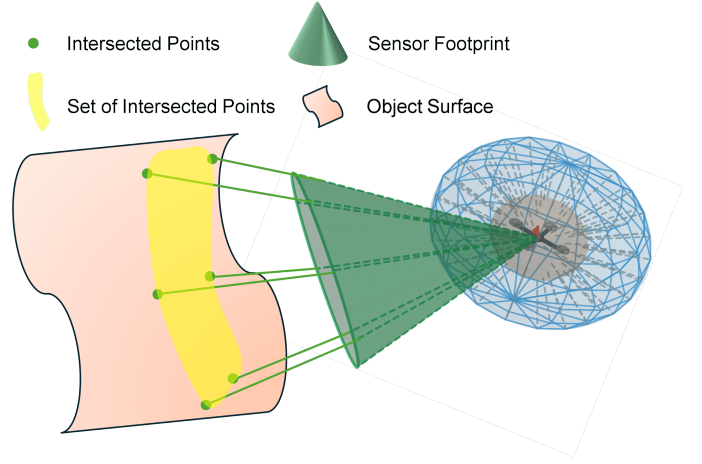


Fig. 4. Illustration of sampling from surface in 3D. The pink surface shows the surface ∂O of the object to be searched. The green cone shows the sensor footprint $\gamma(w, x(t))$ at some time point t , and a set of rays within the sensor footprint (green cone) are sampled and ray-traced to intersect with the object surface ∂O . The green dots in the yellow area show I_R , the set of intersected points of the rays and the object surface.

$r \in \partial O$ where the ray intersects with the object surface, and we use I_R to denote the set of all those intersected points. We use notation r^i, I_R^i to denote a point and the set of intersected points related to robot i .

2) *Multi-Robot Planning:* Similar to the literature on multi-robot ergodic search [9], [17], the footprint ergodic metric for multiple robots \mathcal{E}_{γ}^m (superscript m stands for multi-robot) can be defined based on the average of their time averaged statistics and the information map:

$$\mathcal{E}_{\gamma}^m(\phi, q) = \sum_{\mathbf{k} \in \mathcal{K}} \Lambda_{\mathbf{k}} \left(\frac{1}{N} \sum_{i \in I_N} c_{\gamma, \mathbf{k}}^i - \phi_{\mathbf{k}} \right)^2 \quad (26)$$

In other words, \mathcal{E}_{γ}^m uses the term $\frac{1}{N} \sum_{i \in I_N} c_{\gamma, \mathbf{k}}^i$ to replace the $c_{\gamma, \mathbf{k}}$ term in Eq. 4.

In addition, the inter-robot collision avoidance constraints need to be enforced.

$$\|x^i(t) - x^j(t)\| \geq h_1, \forall i, j \in I, i \neq j \quad (27)$$

where $\|\cdot\|$ denotes the L_2 norm.

To ensure safety, we also impose the following constraint so that the robot stays within a certain distance range, neither too close to nor too far from, the target to be tracked.

$$h_2 \geq \|x^i(t) - r^i(t)\| \geq h_3, \forall i \in I, \forall r^i(t) \in I_R^i(t) \quad (28)$$

where $r^i(t)$ is a sampled point from the object surface that are covered by the sensor as aforementioned.

Problem 2 (MA-ETO-DF). Given an object O , an information map ϕ , the goal of the Multi-Robot Ergodic Trajectory Optimization with Dynamic sensor Footprint (MA-ETO-DF) problem is to find a set of dynamically feasible trajectories

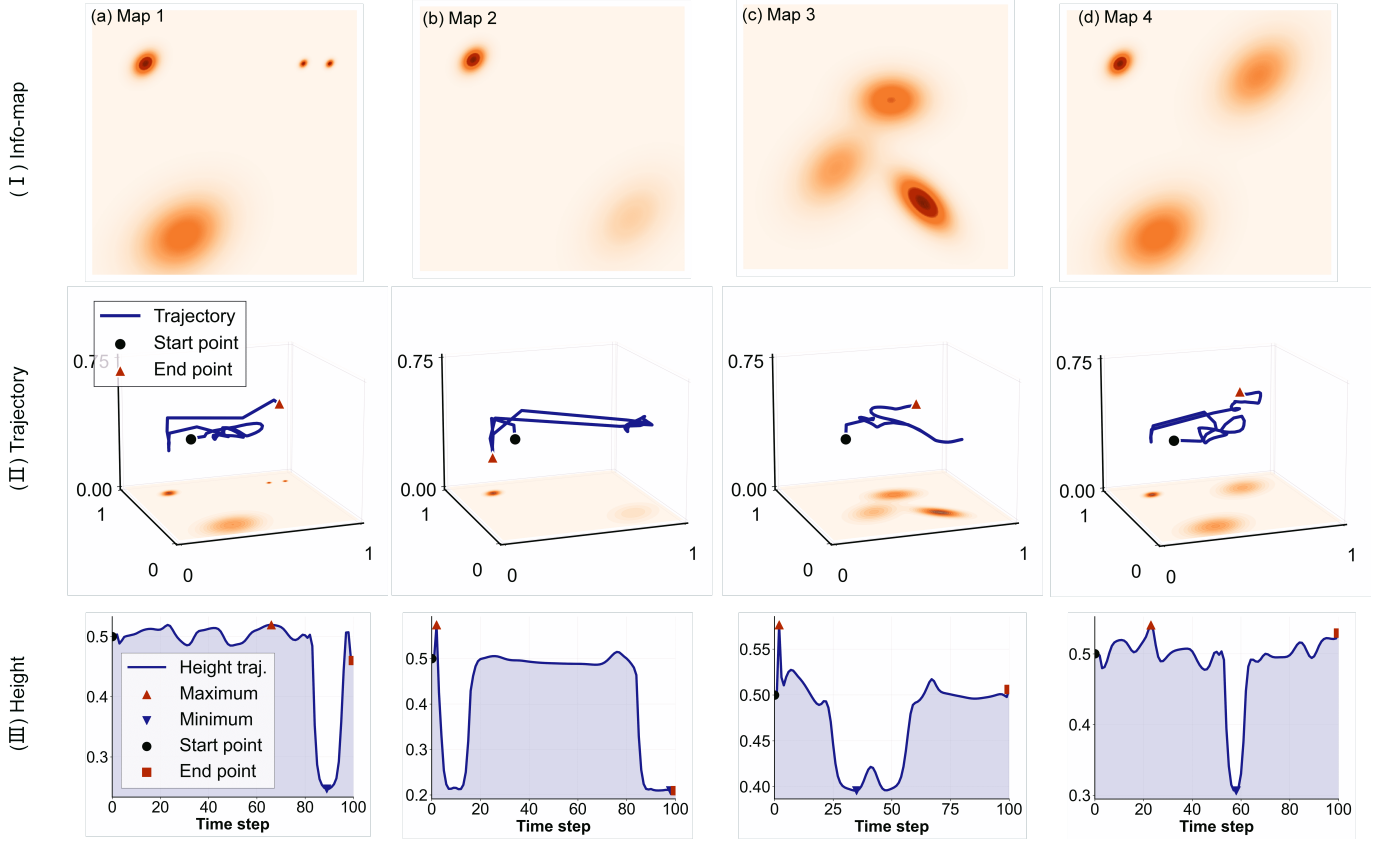


Fig. 5. The experimental results in four different information maps. The first row (I) shows four information maps with various regions with widespread and concentrated information. Row (II) visualizes the planned trajectories. Row (III) shows the corresponding height value (z coordinates) of the robot along the planned trajectories by our FEO. Our FEO can adapt the sensor footprint and the flying height of the robot based on the information map.

$\{x^i | i \in I\}$, one for each robot, that minimizes the footprint ergodic metric $\mathcal{E}_\gamma^m(\phi, x)$ and the accumulated control effort:

$$\min_{x^i, u^i} \mathcal{E}_\gamma^m(\phi, x) + \sum_{i \in I} \int_0^T u^{iT}(t) R u^i(t) dt \quad (29)$$

$$s.t. (3b), (3c), (27), (28) \quad (30)$$

The proposed FEO can be directly applied to solve this MA-ETO-DF problem by incorporating more inequality constraints into the Lagrangian.

V. EXPERIMENTAL RESULTS

A. Experimental Settings

1) *Dynamics and Parameters*: Unless otherwise specified, we consider a workspace $\mathcal{W} = [0, 1] \times [0, 1] \times [0, 1]$. We use the dynamics of a single integrator and a quadrotor in our tests, where the quadrotor dynamics is the same as in [39]. The control u consists of four parameters: roll, pitch, yaw, and thrust. The parameters of the quadrotor dynamics are from Crazyswarm2 [40]. We use the following control limits: roll $\in [-0.4, 0.4]$, pitch $\in [-0.4, 0.4]$, yaw $\in [-3, 3]$, thrust $\in [0, 0.55]$ and the height limit of the drone is $f_h(x) \in [0.1, 0.5]$. The number of samples is $M = 25$ in Eq. 22 when computing $\mathcal{E}_\gamma^m(\phi, x)$. We use the sensor footprint as mentioned in Example 1 with $k_h = 0.25$ by default for the first few

experiments with 2D information maps. We use 10×10 terms when computing the Fourier coefficients.

2) *Baseline Methods*: : Baseline 1 plans trajectories by optimizing the original ergodic metric [6] as mentioned in Eq. 2. Baseline 2 is a variant of our proposed algorithm where the drone has a fixed distance to the information map, so that the corresponding sensor footprint has a fixed size. We vary this footprint size in Baseline 2 in our experiments.

B. Different Maps

Here, we use the quadrotor dynamics and test with various information maps to compare our FEO with the baselines. The total duration of the search is 10 seconds, and the time step is 0.1 seconds. The information maps are shown in the first row of Fig. 5, where Map 1 and 2 have both widely spread information and densely concentrated peaks, while Map 3 only has widely spread information. Map 4 modifies Map 1 and Map 2 with more widely spread information. The trajectories planned by our FEO are shown in the second row, while the flying heights of the robot along the trajectories are shown in the third row. Fig. 5 shows that, our FEO can navigate the robot to fly close to the regions with dense information and fly far away from the regions with widely spread information, by considering the dynamic sensor footprint that varies with the robot states.

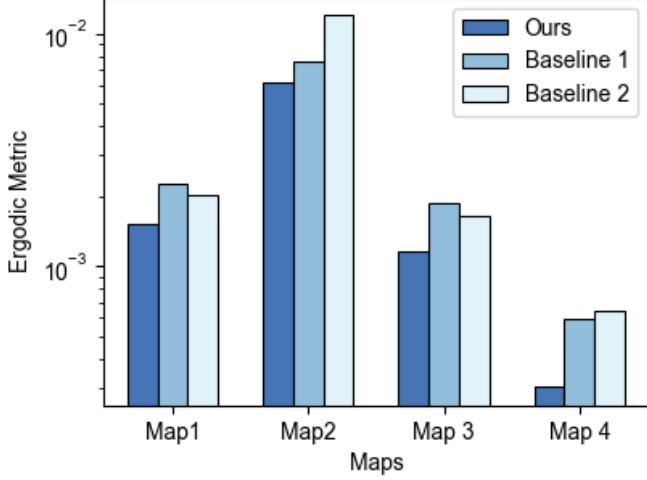


Fig. 6. The corresponding ergodicity of our FEO and the baselines in four maps shown in Fig. 5. Our FEO achieves better (smaller) ergodicity in comparison with the baselines in all maps.

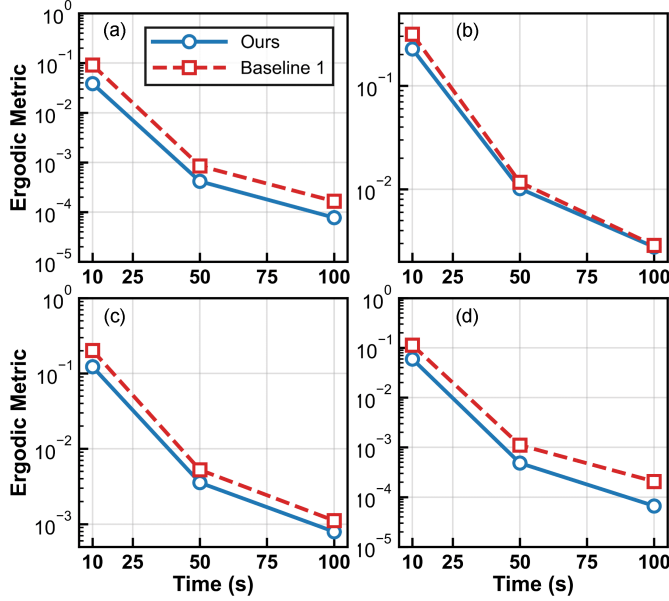


Fig. 7. The influence of planning horizons $T = 10, 50, 100$. As the time horizon increases, all methods, including ours, achieve better ergodicity.

Fig. 6 shows the corresponding ergodicity of our FEO and the baselines in these 4 maps. We plot the footprint ergodicity (Eq. 6) for Baseline 2 and ours, while plotting the conventional ergodicity (Eq. 2) for Baseline 1. Our FEO achieves lower ergodicity than the two baselines, indicating the benefits of planning with dynamic sensor footprints that can dynamically adjust their sizes.

C. Different Planning Horizons

We then test the influence of planning horizons $T \in \{10, 50, 100\}$ on the resulting ergodic metric in the four maps with each time step being 1. The vertical axis is on

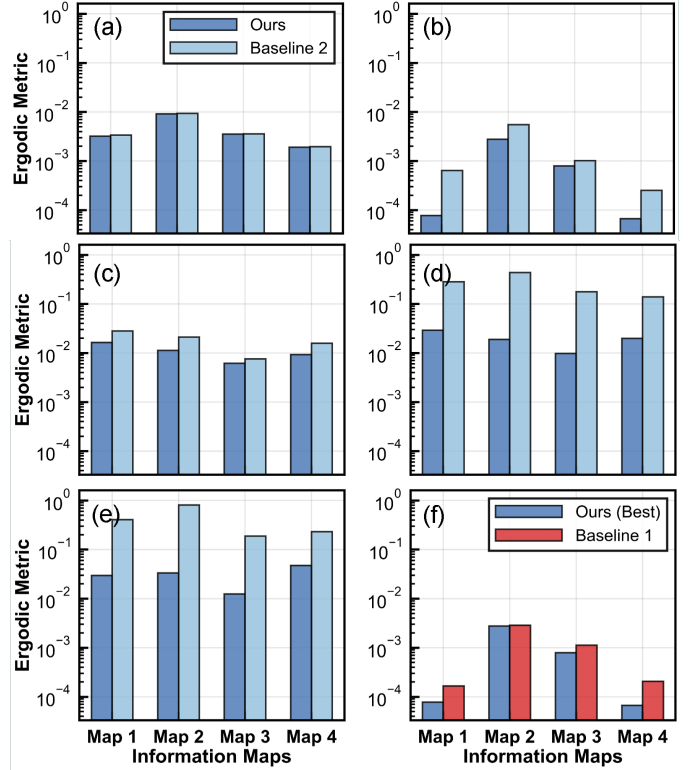


Fig. 8. The resulting ergodic metrics in four maps with various sensor footprint size parameter k_h . Subfigures (a)-(e) show the comparison between our FEO and Baseline 2, where our FEO takes $k_h = 0.01, 0.25, 0.5, 1.0, 1.25$ in (a)-(e) respectively. (f) compares the best result of our FEO among all k_h against Baseline 1. Too large or too small k_h can lead to poor ergodicity for our FEO, while some intermediate value of k_h (e.g. $k_h = 0.25$) results in the best coverage of the information maps in terms of ergodicity.

log-scale. As the planning horizon increases, both our FEO and the baselines find better quality trajectories with smaller ergodicity, which is expected, since in the long term, the planned trajectories tend to have their time-averaged statistics approach the given information map. Additionally, our FEO produces better ergodicity than the baselines due to its ability to plan with dynamic footprints.

D. Different Footprint Sizes

We then test different footprint sizes by varying the parameter k_h in Eq. 4. The planning horizon is $T = 100$ seconds and each time step is 1 second. The ergodic metric comparison between our FEO and the baselines are shown in Fig. 8, and the time-averaged statistics of the footprint trajectories are shown in Fig. 9. All sub-figures in Fig. 8 share the same value range in their vertical axes. We can observe from Fig. 8 that, too large or too small k_h can lead to poor ergodicity, while some intermediate value of k_h (e.g. $k_h = 0.25$) results in the best coverage of the information maps in terms of ergodicity. Furthermore, considering the sensor footprint as a fixed size circle as in Baseline 2 can lead to poor ergodicity compared to our FEO. Our FEO also achieves better ergodicity compared to Baseline 1, if the sensor footprint k_h is properly chosen.

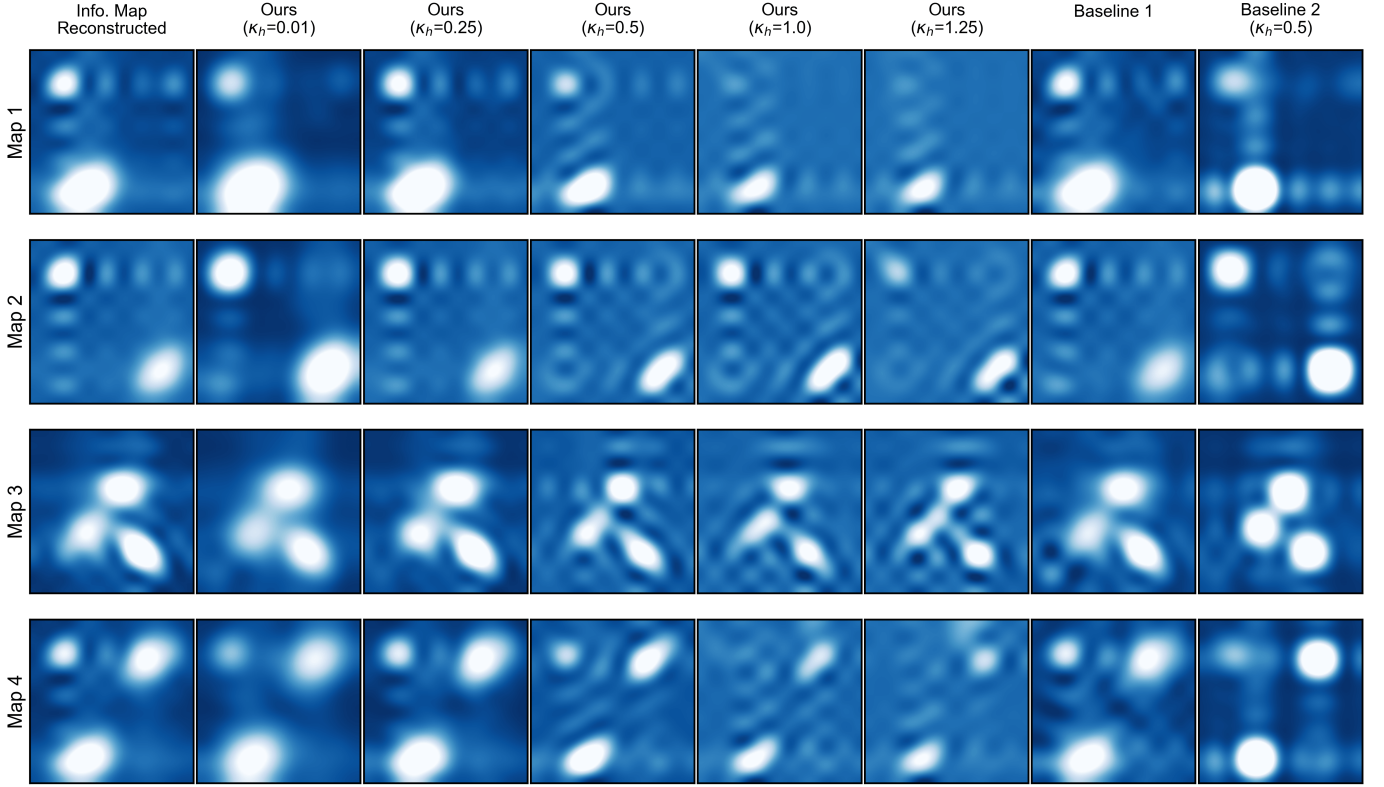


Fig. 9. Comparison between the reconstructed information maps using 10×10 Fourier coefficients and the time-averaged statistics of the sensor footprint with varying footprint size parameters k_h . The first column shows the reconstructed information map. The 2nd to the 5th column shows our FEO with various k_h values. The last two columns show the baselines. The color bar represents the probability density among the maps where white areas have higher information density. An intermediate value of k_h often leads to a time-averaged statistics that is most visually similar to the reconstructed information map.

The time-averaged statistics in Fig. 9 further verify the results. Here, the row shows the reconstructed information map using 10×10 Fourier coefficients. For a large k_h , our FEO has a relatively large footprint and tends to capture coarse information. As shown in Map 1 with $k_h = 1.25$, for example, the time-averaged statistics looks obviously different from the desired reconstructed information map. For a small k_h , our FEO can capture detailed information but may not be efficient for wide spread information, which can be observed from Map 2 with $k_h = 0.01$ and $k_h = 0.25$ by comparing them against the information map reconstructed.

E. Simulation of Multi-Robot in 3D

We use the single-integrator dynamics in this test to plan trajectories for four robots to ergodically coverage an object in 3D in simulation by solving Problem 2. We represent the 3D object using a point cloud in the 3D workspace. Fig. 10(a) shows the object to be covered, and (b) shows the results. In this test, we vary the fixed circle size in Baseline 2 for comparison and our FEO achieves better results than Baseline 2 due to its ability to adjust the sensor footprint size dynamically.³ Fig. 10(c) shows the planned trajectories of the

³We do not consider Baseline 1 in this test since Baseline 1 considers the robot sensor footprint as a point and the object is represented by a point cloud, which makes it very unlikely for two points (one for the robot, the other from the object) to perfectly meet each other.

robots.

F. Real Robots Experiments

1) *System Description*: We use the quadrotor dynamics in all real robot tests. The experimental platform consists of Crazyflie 2.1 micro aerial vehicles [41], which are controlled using the Crazyswarm2 framework [40] integrated with ROS2 [42]. Each quadrotor is equipped with a downward-facing or a forward-facing LED indicator to visualize its sensor footprint during the robot motion. The experiments are conducted within a motion capture system.

2) *Single Robot*: The first test environment is a 2D workspace of size 4.0×4.0 meters with a single drone that seeks to ergodically cover a 2D information map. The flying height of the drone is limited to $[0, 1]$ meters. The planning horizon is 10 seconds with each time step being 0.1. Fig. 1 and 11 show the test setting and some snapshots of the robot motion. We place a few items on the ground in the test area to indicate the information distribution. The robot first flies high to cover the wide spread information with a coarse sensor footprint. After a while, the robot flies to the information peak and lowers its attitude, as shown in Fig. 1(b), in order to cover the dense information with a fine sensor footprint.

3) *Multiple Robots*: Finally, we use 2 drones to cover a chair in 3D space as shown in Fig. 12. The chair is represented by a point cloud which is pre-scanned before the planning

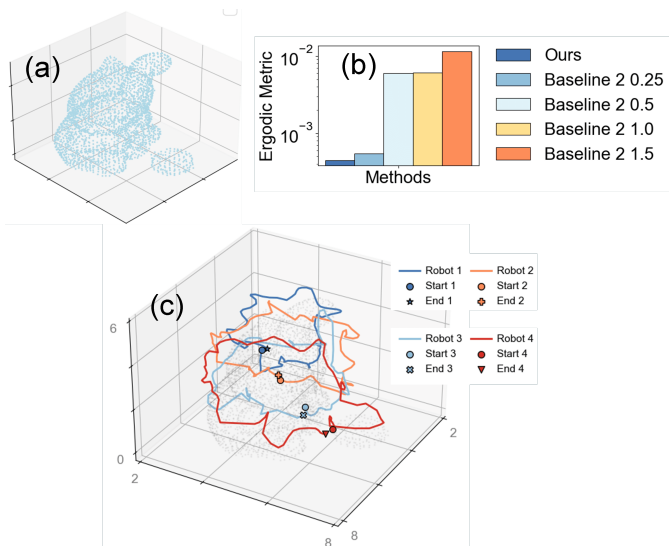


Fig. 10. Simulation with four robots to cover an object in 3D. (a) shows the point cloud representation of the object, a 3D cat model. (b) shows corresponding ergodic metrics of our FEO and Baseline 2 with various k_h . (c) shows the trajectories of the robots in 3D.

starts. Each drone is equipped with a forward-facing LED to illustrate the sensor footprint. The workspace is of size $3.0 \times 3.0 \times 2.0$ meters. The planning horizon is 20 seconds with each time step being 0.1. As shown in the snapshots, the two robots circle around the chair so that their forward-pointing LED can ergodically cover the target object.

VI. CONCLUSIONS AND FUTURE WORK

This paper explores Ergodic Trajectory Optimization with Dynamic sensor Footprints (ETO-DF) and introduces a new footprint ergodic metric that considers the dynamic sensor footprint. We formulate a corresponding Optimal Control Problem (OCP), rewrite it into standard Bolza form, and apply the Pontryagin minimum principle to derive the local optimality conditions for this OCP. We also provide a numerical approach FEO to compute the proposed footprint ergodic metric and leverage Lagrangian optimization to solve the problem. We extend our approach to handle multi-robot and 3D objects. We evaluate our FEO and compare it against baselines in various maps, simulations and real quadrotor experiments. The results verify that, our FEO can plan trajectories for the robots by considering their varying sensor footprints so as to better cover the information map ergodically.

For future work, one can consider dynamic sensor footprints in dynamically changing information maps by integrating the Bayesian filtering framework [38], or consider connectivity maintenance and information communication among the robots [17]. One can also investigate 3D object ergodic coverage using mesh or other representations of the objects.

REFERENCES

[1] Y. Liu and G. Nejat, "Robotic urban search and rescue: A survey from the control perspective," *Journal of Intelligent & Robotic Systems*, vol. 72, no. 2, pp. 147–165, 2013.

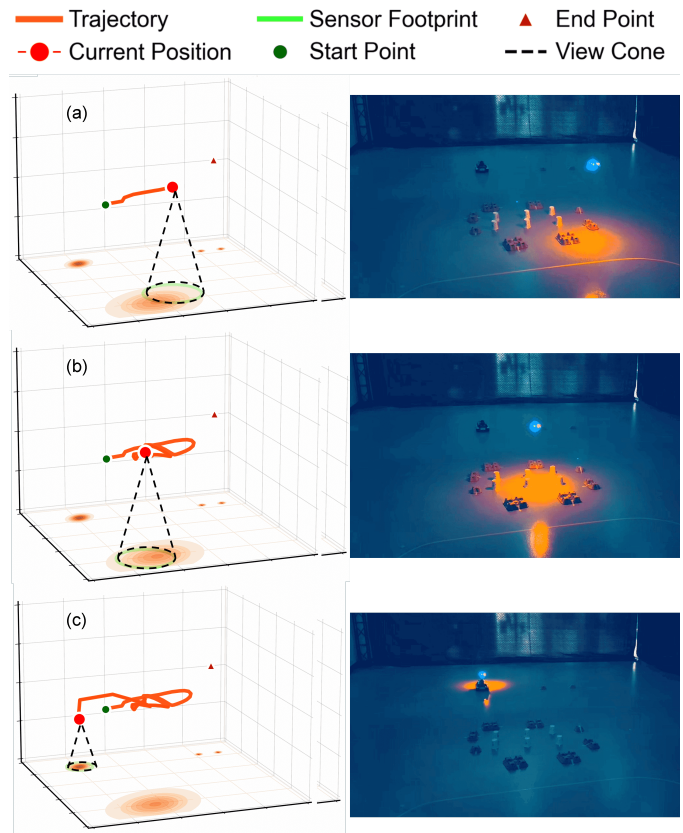


Fig. 11. Snapshots of a drone executing the trajectory planned by FEO in Map 1 shown in Fig. 5. The drone is equipped with a downward-pointing LED to illustrate the sensor footprint. (a)-(c) show the snapshot of the system at time 1.7, 8.3, 9.4 seconds.

[2] A. Mavrommati, E. Tzorakoleftherakis, I. Abraham, and T. D. Murphey, "Real-time area coverage and target localization using receding-horizon ergodic exploration," *IEEE Transactions on Robotics*, vol. 34, no. 1, pp. 62–80, 2017.

[3] B. J. Julian, M. Angermann, M. Schwager, and D. Rus, "Distributed robotic sensor networks: An information-theoretic approach," *The International Journal of Robotics Research*, vol. 31, no. 10, pp. 1134–1154, 2012.

[4] W. Chen and L. Liu, "Pareto monte carlo tree search for multi-objective informative planning," *arXiv preprint arXiv:2111.01825*, 2021.

[5] M. Santos, Y. Diaz-Mercado, and M. Egerstedt, "Coverage control for multirobot teams with heterogeneous sensing capabilities," *IEEE Robotics and Automation Letters*, vol. 3, no. 2, pp. 919–925, 2018.

[6] G. Mathew and I. Mezić, "Metrics for ergodicity and design of ergodic dynamics for multi-agent systems," *Physica D: Nonlinear Phenomena*, vol. 240, no. 4, pp. 432–442, 2011.

[7] L. M. Miller and T. D. Murphey, "Trajectory optimization for continuous ergodic exploration," in *2013 American Control Conference*. IEEE, 2013, pp. 4196–4201.

[8] G. De La Torre, K. Flaßkamp, A. Prabhakar, and T. D. Murphey, "Ergodic exploration with stochastic sensor dynamics," in *2016 American Control Conference (ACC)*. IEEE, 2016, pp. 2971–2976.

[9] I. Abraham and T. D. Murphey, "Decentralized ergodic control: distribution-driven sensing and exploration for multiagent systems," *IEEE Robotics and Automation Letters*, vol. 3, no. 4, pp. 2987–2994, 2018.

[10] E. Ayvali, H. Salman, and H. Choset, "Ergodic coverage in constrained environments using stochastic trajectory optimization," in *2017 IEEE/RSJ International Conference on Intelligent Robots and Systems (IROS)*. IEEE, 2017, pp. 5204–5210.

[11] I. Abraham, A. Prabhakar, and T. D. Murphey, "An ergodic measure for active learning from equilibrium," *IEEE Transactions on Automation*

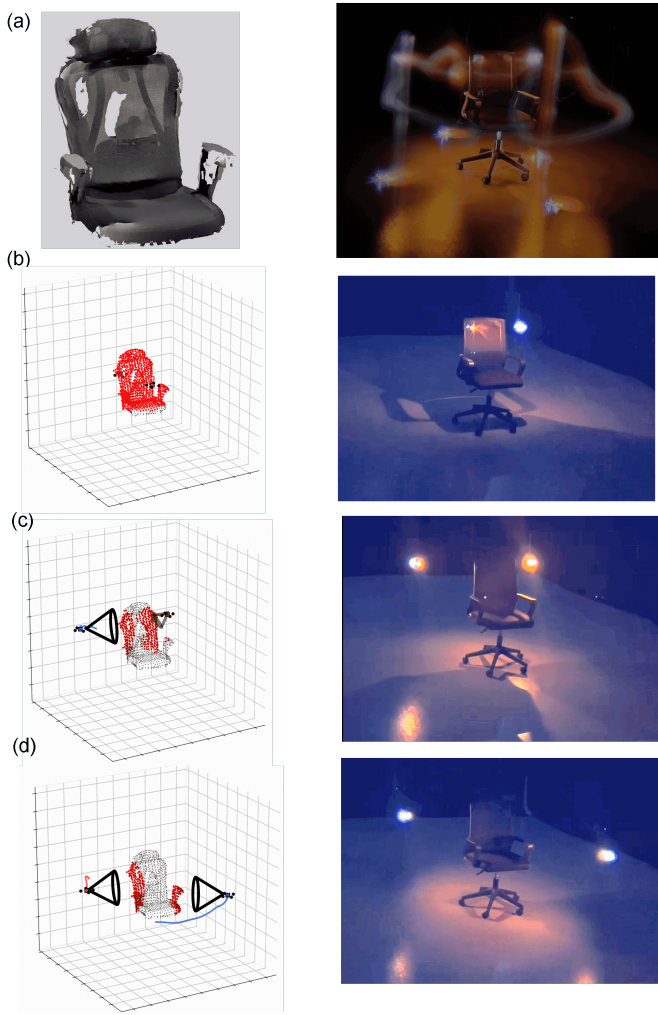


Fig. 12. Snapshots of two drones executing the trajectories planned by FEO to ergodically cover a chair. Each drone is equipped with a forward-facing LED to illustrate the sensor footprint. (a) shows the point cloud of the chair that is pre-scanned. (b)-(d) shows the snapshots of the system at times 0.4, 9.1, 17.5 seconds.

Science and Engineering, 2021.

- [12] M. Sun, A. Gaggari, P. Trautman, and T. Murphey, "Fast ergodic search with kernel functions," *arXiv preprint arXiv:2403.01536*, 2024.
- [13] C. Hughes, H. Warren, D. Lee, F. Ramos, and I. Abraham, "Ergodic trajectory optimization on generalized domains using maximum mean discrepancy," *arXiv preprint arXiv:2410.10599*, 2024.
- [14] S. Ivić, B. Crnković, and I. Mezić, "Ergodicity-based cooperative multiagent area coverage via a potential field," *IEEE transactions on cybernetics*, vol. 47, no. 8, pp. 1983–1993, 2016.
- [15] D. E. Dong, H. Berger, and I. Abraham, "Time-optimal ergodic search: Multiscale coverage in minimum time," *The International Journal of Robotics Research*, p. 02783649241273597, 2024.
- [16] Z. Ren, A. K. Srinivasan, B. Vundurthy, I. Abraham, and H. Choset, "A pareto-optimal local optimization framework for multiobjective ergodic search," *IEEE Transactions on Robotics*, vol. 39, no. 5, pp. 3452–3463, 2023.
- [17] Y. Liu and Z. Ren, "A Probabilistic Measure of Multi-Robot Connectivity and Ergodic Optimal Control," in *Proceedings of Robotics: Science and Systems*, Los Angeles, CA, USA, Jun. 2025. [Online]. Available: https://rap-lab.github.io/documents/publications/2025_RSS_IMEC_YongceLiu_cam.pdf
- [18] S. Shetty, J. Silvério, and S. Calinon, "Ergodic exploration using tensor train: Applications in insertion tasks," *IEEE Transactions on Robotics*, vol. 38, no. 2, pp. 906–921, 2021.
- [19] D. Dong, A. Xu, G. Gutow, H. Choset, and I. Abraham, "Ergodic exploration over meshable surfaces," *arXiv preprint arXiv:2503.05026*, 2025.
- [20] C. Bilaloglu, T. Löw, and S. Calinon, "Tactile ergodic control using diffusion and geometric algebra," *arXiv preprint arXiv:2402.04862*, 2024.
- [21] —, "Whole-body ergodic exploration with a manipulator using diffusion," *IEEE Robotics and Automation Letters*, vol. 8, no. 12, pp. 8581–8587, 2023.
- [22] B. Reily and H. Zhang, "Team assignment for heterogeneous multi-robot sensor coverage through graph representation learning," in *2021 IEEE International Conference on Robotics and Automation (ICRA)*. IEEE, 2021, pp. 838–844.
- [23] X. Wang, J. Xu, C. Gao, Y. Chen, J. Zhang, C. Wang, Y. Ding, and B. M. Chen, "Sensor-based multi-robot coverage control with spatial separation in unstructured environments," in *2024 IEEE International Conference on Robotics and Automation (ICRA)*. IEEE, 2024, pp. 10 623–10 629.
- [24] B. Davis, I. Karamouzas, and S. J. Guy, "C-opt: Coverage-aware trajectory optimization under uncertainty," *IEEE Robotics and Automation Letters*, vol. 1, no. 2, pp. 1020–1027, 2016.
- [25] C. Mostegel, J. Ye, Y. Luo, and Y. Liu, "Overlap displacement error: Are your slam poses map-consistent?" in *2021 IEEE/RSJ International Conference on Intelligent Robots and Systems (IROS)*. IEEE, 2021, pp. 5336–5343.
- [26] M. Nieuwenhuisen and S. Behnke, "Search-based 3d planning and trajectory optimization for safe micro aerial vehicle flight under sensor visibility constraints," in *2019 International Conference on Robotics and Automation (ICRA)*. IEEE, 2019, pp. 9123–9129.
- [27] B. Hepp, M. Nießner, and O. Hilliges, "Plan3d: Viewpoint and trajectory optimization for aerial multi-view stereo reconstruction," *ACM Transactions on Graphics (TOG)*, vol. 38, no. 1, pp. 1–17, 2018.
- [28] G. Best, O. M. Cliff, T. Patten, R. R. Mettu, and R. Fitch, "Decmets: Decentralized planning for multi-robot active perception," *The International Journal of Robotics Research*, vol. 38, no. 2-3, pp. 316–337, 2019.
- [29] T. Patten, M. Zillich, R. Fitch, M. Vincze, and S. Sukkarieh, "Viewpoint evaluation for online 3-d active object classification," *IEEE Robotics and Automation Letters*, vol. 1, no. 1, pp. 73–81, 2015.
- [30] R. Agishev, T. Petříček, and K. Zimmermann, "Trajectory optimization using learned robot-terrain interaction model in exploration of large subterranean environments," *IEEE Robotics and Automation Letters*, vol. 7, no. 2, pp. 3365–3371, 2022.
- [31] Y. Cai, Y. Ou, and T. Qin, "Improving slam techniques with integrated multi-sensor fusion for 3d reconstruction," *Sensors*, vol. 24, no. 7, p. 2033, 2024.
- [32] M. Zwick, M. Gerdt, and P. Stütz, "Enhancing detection performance through sensor model-based trajectory optimization for uavs," in *2021 IEEE/AIAA 40th Digital Avionics Systems Conference (DASC)*. IEEE, 2021, pp. 1–10.
- [33] Z. Tang and U. Ozguner, "Motion planning for multitarget surveillance with mobile sensor agents," *IEEE Transactions on Robotics*, vol. 21, no. 5, pp. 898–908, 2005.
- [34] H. Coffin, I. Abraham, G. Sartoretto, T. Dillstrom, and H. Choset, "Multi-agent dynamic ergodic search with low-information sensors," in *2022 International Conference on Robotics and Automation (ICRA)*. IEEE, 2022, pp. 11 480–11 486.
- [35] S. A. Sadat, J. Wawerla, and R. Vaughan, "Fractal trajectories for online non-uniform aerial coverage," in *2015 IEEE international conference on robotics and automation (ICRA)*. IEEE, 2015, pp. 2971–2976.
- [36] E. Galceran and M. Carreras, "Efficient seabed coverage path planning for asvs and auvs," in *2012 IEEE/RSJ International Conference on Intelligent Robots and Systems*. IEEE, 2012, pp. 88–93.
- [37] F. Stache, J. Westheider, F. Magistri, C. Stachniss, and M. Popović, "Adaptive path planning for uavs for multi-resolution semantic segmentation," *Robotics and Autonomous Systems*, vol. 159, p. 104288, 2023.
- [38] L. M. Miller, Y. Silverman, M. A. MacIver, and T. D. Murphey, "Ergodic exploration of distributed information," *IEEE Transactions on Robotics*, vol. 32, no. 1, pp. 36–52, 2015.
- [39] C. Llanes, Z. Kakish, K. Williams, and S. Coogan, "Crazysim: A software-in-the-loop simulator for the crazyflie nano quadrotor," in *Int. Conf. Rob. Aut.*, 2024.
- [40] J. A. Preiss, W. Honig, G. S. Sukhatme, and N. Ayanian, "Crazyswarm: A large nano-quadcopter swarm," in *2017 IEEE International Conference on Robotics and Automation (ICRA)*. IEEE, 2017, pp. 3299–3304.
- [41] W. Giernacki, M. Skwierczyński, W. Witwicki, P. Wroński, and P. Kozierski, "Crazyflie 2.0 quadrotor as a platform for research and

education in robotics and control engineering,” in *2017 22nd International Conference on Methods and Models in Automation and Robotics (MMAR)*, 2017, pp. 37–42.

- [42] S. Macenski, T. Foote, B. Gerkey, C. Lalancette, and W. Woodall, “Robot operating system 2: Design, architecture, and uses in the wild,” *Science robotics*, vol. 7, no. 66, p. eabm6074, 2022.